Two-Stage Robust Optimization for Resilient Operation of Microgrids Considering Hierarchical Frequency Control Structure

Mohiti, Maryam; Monsef, Hassan; Anvari-Moghaddam, Amjad; Lesani, Hamid

Published in:
I E E E Transactions on Industrial Electronics

DOI (link to publication from Publisher):
10.1109/TIE.2019.2956417

Publication date:
2020

Document Version
Accepted author manuscript, peer reviewed version

Two-Stage Robust Optimization for Resilient Operation of Microgrids Considering Hierarchical Frequency Control Structure

Maryam Mohiti, Hassan Monsef, Amjad Anvari-Moghaddam, S*enior Member, IEEE*, Hamid Lesani

***Abstract*— Following a major outage in the main grid due to natural disasters, microgrids (MGs) have the ability to disconnect from the main grid and provide electricity to their consumers. However, integration of power electronic-based generation units and small-scale energy resources into MGs reduces the system inertia. Therefore, frequency deviations arising from loss of grid power or fluctuations of renewable energy resources and loads, should be managed. In this paper, a two-stage robust day-ahead optimization model for resilient operation of MGs is proposed in which hierarchical frequency control structure of the MG is precisely formulated. Based on this model, the operation cost of MG is minimized while sufficient primary and secondary reserves are scheduled to restrict frequency deviations and avoid load shedding under the worst-case realization of islanding events. A column-and-constraint generation (C&CG) algorithm is utilized to efficiently solve the problem. Numerical cases on a test system show the effectiveness of the proposed model and the solution algorithm. The obtained results verify that by applying the proposed model, operating cost of MG is minimized while the frequency deviation and load shedding can be successfully managed during islanding events.**

***Index Terms*— Frequency control, microgrid optimal operation, resilient microgrid, two-stage robust optimization, uncertainty.**

NOMENCLATURE

Indices and Sets

$e \in ESS$	Index/set of energy storage system (ESS)
$j \in DG$	Index/set of distributed generation (DG)
$n \in N$	Index/set of buses
$p \in PV$	Index/set of photovoltaic system (PV)
pre/pri/sec	Index of previous /primary/secondary interval in MG frequency control
$t \in \Omega_T$	Index/set of time

Symbols

$\overline{(\bullet)} / \underline{(\bullet)}$	Maximum/minimum bounds of variable $(\bullet)$
$\widetilde{(\bullet)} / \widehat{(\bullet)}$	Value / Deviation of uncertain variable $(\bullet)$
$(\bullet)^*$	Optimal value of variable $(\bullet)$

Manuscript received March 10, 2019; revised May 01, August 01, and October 04, 2019; accepted November 11, 2019.

M. Mohiti, H. Monsef, and H.Lesani are with the Department of Electrical and Computer Engineering, University of Tehran, Tehran, Iran. (email: m.mohiti, hmonsef, lesani @ut.ac.ir).

A. Anvari-Moghaddam is with the Department of Energy Technology, Aalborg University, Aalborg, Denmark (e-mail: aam@et.aau.dk).

I. INTRODUCTION

WITH the significant effect of weather-related incidents (WRIs) on power systems, resiliency of such systems has attracted growing attention. Different definitions for resiliency have been discussed in literature [1 , 2]. National Infrastructure Advisory Council introduces four main resiliency features: robustness, resourcefulness, rapid recovery, and adaptability [3]. Robustness is defined as the ability to withstand low-probability but severe events. Resourcefulness implies effective management of WRI and prioritizing resources while rapid recovery and adaptability refers to the emergency plans and enhancing the system resiliency for future events, respectively. According to [4], power system resiliency can be studied from short-term and long-term perspectives. Short-term resiliency consists of actions performed prior to, during and, after an incident. To this end, resiliency features such as robustness (prior to the incident), resourcefulness (during the incident), and recovery (after the incident) are investigated. In long-term perspective, the adaptability of the system to future events is studied.

Microgrids may have the capability of improving system resiliency by supplying the loads locally and reducing the possibility of load shedding [5]. In case of emergency, MGs can be isolated from the faulty part of the distribution network and sustain the power supply through optimal operation of available resources. This ability makes MGs less vulnerable to natural disasters.

Many research works have been conducted to enhance the resiliency of power system through MGs. In [6] a strategy is presented to restore critical loads by using MGs as an emergency source. The proactive operation strategy presented in [7] deploys energy storage systems for enhancing resiliency of MGs. Authors of [8] have considered feasible islanding and survivability of critical loads in grid-connected and islanding operations of a MG to improve the resiliency of a multi-MG system. Authors of [9] introduce an outage management scheme to enhance the resiliency of a multi-MG system against natural disasters. A two-stage stochastic programming approach is presented in [10] for optimal scheduling of a resilient MG. Likewise, [11] presents a stochastic framework for optimal management of MG during unscheduled islanding operation, started by incidents. In [12] a proactive resilience-

oriented framework for management of MGs through windstorms is presented in which the number of line outages and load curtailment at the event onset is minimized. Authors of [13] present a resiliency-oriented MG scheduling model in which load curtailment is minimized in islanded periods while operation cost is minimized in grid-connected.

In the above studies different features of resiliency enhancement have been investigated. However, following a severe disturbance, which causes mismatch between power supply and demand, frequency is exposed to severe deviation. Besides, in MGs due to the large share of renewable energy sources (RESs), conventional generators are replaced by converter-interfaced generations, therefore, the inertia of the system is reduced, significantly. This means that MGs are more vulnerable to frequency deviations [14]. Such situation can be even worse in islanded MGs where the power mismatch ratio to the capacity of MG is high. Frequency deviations can lead to extensive load tripping and increase the possibility of system damage. On the other hand, there is a tight coupling between reserve scheduling and frequency security of MG [15]. Thus, in resilient operation of MG both frequency control structure and reserve scheduling should be considered.

In this paper, a two-stage robust day-ahead optimization model for resilient operation of MGs is proposed and complemented by an effective hierarchical frequency control structure. The proposed model aims to minimize the total operation cost of MG while sufficient primary and secondary reserve are scheduled to restrict frequency deviations and avoid load shedding under the worst-case realization of islanding events. As frequency control structure of MGs plays a key role in the proposed model, load frequency dependency is considered in both primary and secondary control intervals. To solve the proposed robust model, column-and-constraint generation algorithm is introduced which decomposes the two-stage robust optimization problem into a master and sub-problem. The main contributions of this paper can be summarized as follow:

- A novel two-stage robust optimization framework with a resiliency enhancement perspective is proposed in which the hierarchical frequency control structure of MGs is modeled precisely.
- In the proposed day-ahead scheduling model, the energy and reserve in primary and secondary intervals are optimized to enhance the resiliency of the MG while keeping the primary and secondary frequency deviations in permissible range.
- The reference set-points of DGs in the secondary control interval are optimized through a well-organized mixed integer linear programming (MILP).

The rest of the paper is organized as follow. In section II a general description of MGs control structure is presented. Section III introduces the problem formulation in grid-connected and islanded operation mode. The robust model formulation and solution algorithm are presented in section IV. The results are brought in section V. Finally, the paper is concluded in section VI.

II. General Description of MG Control System

A. Hierarchical control of MGs

Similar to the power systems, the control structure of MGs can be categorized into three hierarchical levels, namely primary, secondary, and tertiary control [16] as shown in Fig. 1. The primary control which responds to system dynamics, is carried out locally for DGs and generally consists of droop control and inner control loops. The main idea of this control level is based on the droop control method and can be presented by the following equations [17]:

$$f_t = f^{ref} - mp_j (P_{j,t}^{DG} - P_{j,t}^{DG,ref}) \quad (1)$$

$$V_{j,t} = V_{j,t}^{ref} - mq_j (Q_{j,t}^{DG} - Q_{j,t}^{DG,ref}) \quad (2)$$

where, f, f^{ref}, V, and V^{ref} are the MG frequency, frequency reference value, voltage, and voltage reference value of the converter. Meanwhile, P^{DG}/Q^{DG}, $P^{DG,ref}/Q^{DG,ref}$, and mp/mq are active/reactive power output, active/reactive power reference values of DGs, and droop gains of the primary frequency/voltage controllers. In Fig. 1, deviations in the MG active and reactive power change the output current and voltage. The frequency and voltage droop controllers which sense the deviations, automatically activate primary reserves and/or inject reactive power to mitigate frequency and voltage deviations. It should be noted that the compensated frequency and voltage signals are regulated in the converter's inner current (G_I) and voltage (G_V) controllers such that the final reference voltage phasor is produced and sent to the gating algorithm of the voltage source converter (VSC). However, execution of the primary control level by local controllers may introduce steady-state errors in system frequency and bus voltages. The secondary control closely works with the local controllers to restore the frequency and voltage to their nominal values. As shown in Fig. 1 at the secondary control level, MG central controller (MGCC) restores the frequency and voltage by regulating the set-points of DGs. The secondary control loop represents relatively slower response times compared to primary controller. Tertiary control is in charge of regulating exchanged power with the external grid and economic management of MG. This control level which behaves as an

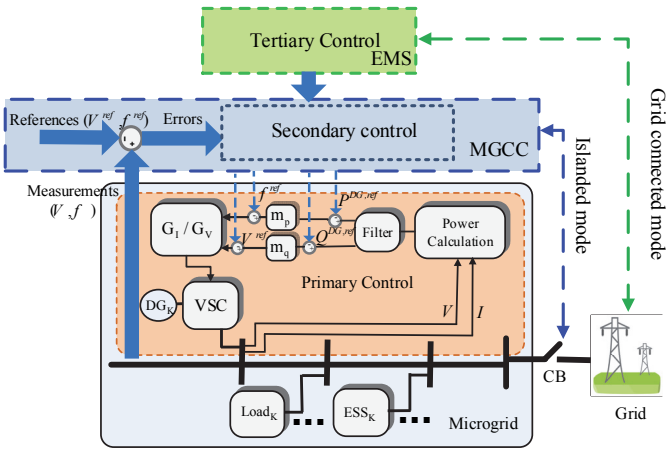

Fig. 1. Hierarchical control of MG

energy management system generates optimal set-points for lower-level control layers. It should be mentioned that the focus in the proposed day-ahead scheduling is given to the frequency droop control of converter-interfaced DGs assuming that the reactive power regulation is performed in a decoupled way, thus the voltage regulation requirements could be satisfied locally [18, 19]. For further information see Appendix A.

B. Primary and secondary interval formulation

In both primary and secondary intervals, the power deviations of converter-interfaced DGs according to their frequency-droop characteristic can be presented as (3) [20]. Here, it is assumed that RESs do not participate in the frequency control of MG and the oscillation modes are damped out.

$$\sum_{j\in DG}\Delta P_{j,t}^{DG}=\sum_{j\in DG}\Delta P_{j,t}^{DG,ref}-\Delta f_t\left(D_t+\sum_{j\in DG}\frac{u_{j,t}}{mp_j}\right) \tag{3}$$

where, u is a binary variable indicating commitment state of DGs. In this paper, frequency-dependent loads are modeled and their elasticity (D) is calculated as follows:

$$D_t=\sum_{n\in N}P_{n,t}^{D}\Big/f^{ref} \tag{4}$$

where, P^D is the demand of MG. Since the duration of primary control is short (e.g., 30 seconds), the commitment states and reference power set points of DGs cannot be altered; thus, in the primary control level, both the commitment state and reference power set points of DGs are constant and the same as the previous interval which can be expressed as follows:

$$\Delta P_{j,t}^{DG,ref,pri}=0,\quad u_{j,t}^{pri}=u_{j,t}^{pre} \tag{5}$$

According to (5), equation (3) for the primary interval can be rewritten as follows:

$$\sum_{j\in DG}\left(P_{j,t}^{DG,pri}-P_{j,t}^{DG,pre}\right)=0-\Delta f_t^{pri}\left(D_t+\sum_{j\in DG}\frac{u_{j,t}^{pri}}{mp_j}\right) \tag{6}$$

Therefore, the frequency excursions of the primary interval can be calculated as follows:

$$\Delta f_t^{pri}=\frac{-\sum_{j\in DG}P_{j,t}^{DG,pri}-P_{j,t}^{DG,pre}}{D_t+\sum_{j\in DG}\frac{u_{j,t}^{pri}}{mp_j}} \tag{7}$$

In the secondary interval which usually lasts for several minutes (e.g., 15 minutes), there is enough time to change the commitment states and power set points of DGs. Thus, equation (3) in the secondary interval can be written as:

$$\sum_{j\in DG}(P_{j,t}^{DG,\sec}-P_{j,t}^{DG,pri})=\sum_{j\in DG}(P_{j,t}^{DG,ref,\sec}-P_{j,t}^{DG,ref,pri})$$
$$-(D_t+\sum_{j\in DG}\frac{u_{j,t}^{\sec}}{mp_j})(f_t^{\sec}-f_t^{pri}) \tag{8}$$

By substitution of $P_{j,t}^{DG,pri}$ from (6) into (8):

$$\sum_{j\in DG}P_{j,t}^{DG,\sec}=\sum_{j\in DG}P_{j,t}^{DG,ref,\sec}$$
$$-(D_t+\sum_{j\in DG}\frac{u_{j,t}^{\sec}}{mp_j})(f_t^{\sec}-f_t^{pre}) \tag{9}$$

Thus, the secondary frequency excursions can be obtained as:

$$\Delta f_t^{\sec}=\frac{-\sum_{j\in DG}(P_{j,t}^{DG,\sec}-P_{j,t}^{DG,ref,\sec})}{D_t+\sum_{j\in DG}\frac{u_{j,t}^{\sec}}{mp_j}} \tag{10}$$

For convenience, $P_{j,t}^{DG,ref,\sec}$ is represented by $P_{j,t}^{DG,ref}$ in the rest of the paper.

III. Deterministic Model Formulation

This section presents optimal day-ahead scheduling problem of a MG. To help to understand the proposed model better, first a deterministic approach, in which the operation uncertainties are ignored, is provided.

A. Objective function

The objective function is to minimize total operation cost of the MG considering both normal and islanding modes. The operation cost during the normal mode involves the cost of purchasing power from the external grid, reserve provision cost of DGs, power production cost of DGs, and degradation cost of ESS. Since the islanding mode is resiliency-oriented, only load shedding cost in the primary and secondary control intervals are considered. The objective function is formulated as follows:

$$\begin{aligned}\min\ &\sum_{t\in\Omega_T}\lambda_t^G P_t^G+\sum_{j\in DG}\sum_{t\in\Omega_T}\lambda_j^{RE}\left(R_{j,t}^{DG,pri}+R_{j,t}^{DG,\sec}\right)\\&+\sum_{j\in DG}\sum_{t\in\Omega_T}\left(\lambda_j^{SU}u_{j,t}^{SU}+\left[\alpha_j u_{j,t}+\beta_j P_{j,t}^{DG}\right]+\lambda_j^{SD}u_{j,t}^{SD}\right)\\&+\sum_{e\in ESS}\sum_{t\in\Omega_T}\left(\lambda_e^{ESS}k_{SOC}\left[1-\underline{SOC_e}\right]\right)SOC_{e,t}\\&+\sum_{n\in N}\sum_{t\in\Omega_T}\lambda_t^{shed}\left(P_{n,t}^{LS,pri}+P_{n,t}^{LS,\sec}\right)\end{aligned} \tag{11}$$

where, λ^G/ λ^{RE}, λ^{SU}/ λ^{SD}, λ^{ESS}, and λ^{shed} are the wholesale market/reserve price, start-up/shut-down cost of DG, maintenance cost of ESS, and penalty for load shedding. P^G, R^{DG}, P^{LS}, and u^{SU}/u^{SD} are imported power from external grid, scheduled reserve of DG, curtailed power of MG in islanded mode, and binary variable indicating start-up/shut down of DG. α and β are coefficients of DG's cost function. SOC is state of charge of ESS and k_{SOC} is a parameter related to state of charge of ESS.

B. Constraints of normal operation mode

The constraints of normal operation mode are as follow:

$$\begin{aligned}&P_t^G+\sum_{j\in DG}P_{j,t}^{DG}+\sum_{p\in PV}P_{p,t}^{PV}+\\&\sum_{e\in ESS}\left(P_{e,t}^{dis}-P_{e,t}^{cha}\right)=\sum_{n\in N}P_{n,t}^{D}\end{aligned} \tag{12}$$

$$0 \le P_t^G \le \overline{P^G} \tag{13}$$

$$\underline{P_j^{DG}} u_{j,t} \le P_{j,t}^{DG} + R_{j,t}^{DG,pri} + R_{j,t}^{DG,\sec} \le \overline{P_j^{DG}} u_{j,t} \tag{14}$$

$$P_{j,t}^{DG} - P_{j,t-1}^{DG} \le UR_j \left(1 - u_{j,t}^{SU}\right) + \underline{P_j^{DG}} u_{j,t}^{SU} \tag{15}$$

$$P_{j,t-1}^{DG} - P_{j,t}^{DG} \le DR_j \left(1 - u_{j,t}^{SD}\right) + \underline{P_j^{DG}} u_{j,t}^{SD} \tag{16}$$

$$\sum_{h=t}^{t+UT_j-1} u_{j,h} \ge UT_j u_{j,t}^{SU} \tag{17}$$

$$\sum_{h=t}^{t+DT_j-1} \left(1 - u_{j,h}\right) \ge DT_j u_{j,t}^{SD} \tag{18}$$

$$u_{j,t+1} - u_{j,t} \le u_{j,t+1}^{SU} \tag{19}$$

$$u_{j,t} - u_{j,t+1} \le u_{j,t+1}^{SD} \tag{20}$$

$$u_{j,t+1} - u_{j,t} = u_{j,t+1}^{SU} - u_{j,t+1}^{SD} \tag{21}$$

$$P_{p,t}^{PV} \le \overline{P_{p,t}^{PV}} \tag{22}$$

where, P^{PV} and P^{cha}/P^{dis} are the scheduled power of PV and charged/discharged power of ESS, respectively. UR/DR and UT/DT are the ramp up/down of DG and minimum up/down time of DG. Constraint (12) enforces hourly load balance in the MG. The imported power from the external grid is limited by (13) regarding the capacity of transformer located in the main substation. The scheduled power of DGs is restricted to their upper and lower generation levels by (14). Likewise, ramp up/down limitations of DGs are presented in (15) and (16) while, minimum up/down time limitations are described by (17) and (18), respectively. Concurrent starting-up or shutting-down of DGs are avoided by (19)-(21). In (22), the scheduled power of PVs is restricted to their available generation.

The ESS is modeled by the following constraints:

$$0 \le P_{e,t}^{cha} \le bsc_{e,t} \overline{P_e^{cha}} \tag{23}$$

$$0 \le P_{e,t}^{dis} \le bsd_{e,t} \overline{P_e^{dis}} \tag{24}$$

$$bsc_{e,t} + bsd_{e,t} \le 1 \tag{25}$$

$$SOC_{e,t} = SOC_{e,t-1} - P_{e,t}^{dis} / \eta^d + P_{e,t}^{cha} \eta^c \tag{26}$$

$$\underline{SOC_e} \le SOC_{e,t} \le \overline{SOC_e} \tag{27}$$

where, bsc/bsd and η^c/η^d represent the charge/discharge status and charge/discharge efficiency of ESS, respectively.

C. Constraint of islanding operation mode

Following a WRI, the MG may be islanded from the external grid. In such circumstances, MGCC aims to minimize the total load shedding cost through re-dispatch of DGs using the dedicated hierarchical controllers. The following constraints must be met in the islanding operation mode:

$$P_t^G I_t + \sum_{j \in DG} P_{j,t}^{DG,pri} + \sum_{p \in PV} P_{p,t}^{PV} + \sum_{e \in ESS} \left(P_{e,t}^{dis} - P_{e,t}^{cha}\right) + \sum_{n \in N} P_{n,t}^{LS,pri} = \sum_{n \in N} P_{n,t}^{D} + D_t \Delta f_t^{pri} \tag{28}$$

$$P_t^G I_t + \sum_{j \in DG} P_{j,t}^{DG,\sec} + \sum_{p \in PV} P_{p,t}^{PV} + \sum_{e \in ESS} \left(P_{e,t}^{dis} - P_{e,t}^{cha}\right) + \sum_{n \in N} P_{n,t}^{LS,\sec} = \sum_{n \in N} P_{n,t}^{D} + D_t \Delta f_t^{\sec} \tag{29}$$

$$-\Delta f_t^{pri} \le \overline{\Delta f^{pri}} \tag{30}$$

$$-\Delta f_t^{\sec} \le \overline{\Delta f^{\sec}} \tag{31}$$

$$P_{n,t}^{LS,pri} \le P_{n,t}^{D} \tag{32}$$

$$P_{n,t}^{LS,\sec} \le P_{n,t}^{D} \tag{33}$$

$$\underline{P_{j,t}^{DG}} u_{j,t}^{pri} \le P_{j,t}^{DG,pri} \le \overline{P_{j,t}^{DG}} u_{j,t}^{pri} \tag{34}$$

$$\underline{P_{j,t}^{DG}} u_{j,t}^{\sec} \le P_{j,t}^{DG,\sec} \le \overline{P_{j,t}^{DG}} u_{j,t}^{\sec} \tag{35}$$

$$\underline{P_{j,t}^{DG}} u_{j,t}^{pri} \le P_{j,t}^{DG,ref} \le \overline{P_{j,t}^{DG}} u_{j,t}^{pri} \tag{36}$$

$$\underline{P_{j,t}^{DG}} u_{j,t}^{\sec} \le P_{j,t}^{DG,ref} \le \overline{P_{j,t}^{DG}} u_{j,t}^{\sec} \tag{37}$$

$$P_{j,t}^{DG,pri} - P_{j,t}^{DG,pre} \le R_{j,t}^{DG,pri} + \left(1 - u_{j,t}^{pri}\right) \overline{P_j^{DG}} \tag{38}$$

$$P_{j,t}^{DG,ref} - P_{j,t}^{DG,pre} \le R_{j,t}^{DG,\sec} + \left(1 - u_{j,t}^{\sec}\right) \overline{P_j^{DG}} \tag{39}$$

$$P_{j,t}^{DG,pri} - P_{j,t}^{DG,pre} \le UR_j u_{j,t}^{pri} \tag{40}$$

$$P_{j,t}^{DG,pre} - P_{j,t}^{DG,pri} \le DR_j u_{j,t}^{pri} \tag{41}$$

$$P_{j,t}^{DG,\sec} - P_{j,t}^{DG,pri} \le UR_j u_{j,t}^{pri} + \left(1 - u_{j,t}^{\sec}\right) \overline{P_j^{DG}} \tag{42}$$

$$P_{j,t}^{DG,pri} - P_{j,t}^{DG,\sec} \le DR_j u_{j,t}^{\sec} + \left(1 - u_{j,t}^{pri}\right) \overline{P_j^{DG}} \tag{43}$$

$$P_{j,t}^{DG,pri} - P_{j,t-1}^{DG,pri} \le UR_j u_{j,t-1}^{pri} + \left(1 - u_{j,t}^{pri}\right) \overline{P_j^{DG}} \tag{44}$$

$$P_{j,t-1}^{DG,pri} - P_{j,t}^{DG,pri} \le DR_j u_{j,t}^{pri} + \left(1 - u_{j,t-1}^{pri}\right) \overline{P_j^{DG}} \tag{45}$$

$$P_{j,t}^{DG,\sec} - P_{j,t-1}^{DG,\sec} \le UR_j u_{j,t-1}^{\sec} + \left(1 - u_{j,t}^{\sec}\right) \overline{P_j^{DG}} \tag{46}$$

$$P_{j,t-1}^{DG,\sec} - P_{j,t}^{DG,\sec} \le DR_j u_{j,t}^{\sec} + \left(1 - u_{j,t-1}^{\sec}\right) \overline{P_j^{DG}} \tag{47}$$

where, I is a binary variable indicating islanding status of MG. The total generation and demand should be equal at each control level which is met by (28) and (29). The frequency deviation in the primary and secondary intervals which are obtained by (7) and (10), are kept in the permissible range using constraints (30) and (31). Likewise, constraints (32) and (33) limit the primary and secondary load shedding at each bus of MG to its hourly demand. The set of constraints (34)-(37) limit the DGs' power in primary and secondary intervals as well as reference power set-points of DGs within their lower and upper limits. The constraints described by (38) and (39) are used to adjust the reference power set-points of committed DGs considering the scheduled primary and secondary reserves. Ramp-up and down limitations of DGs are modeled in (40)-(47) to cover primary and secondary intervals and their interactions.

IV. ROBUST MODEL FORMULATION

In practice, MG operational scheduling problem is solved one day in advance and hence, load, renewable generation, and islanding event are uncertain and unknown. In this section, a two-stage robust optimization model is proposed to cope with

the mentioned uncertainties.

A. Uncertainty modeling

In the robust optimization, uncertainties are characterized using appropriate uncertainty sets. Such a set for the MG load (U_D) can be defined as follows:

$$U_D=\left\{\begin{array}{l}\widetilde{P}^D_{n,t}\in R^+\left|\underline{\Gamma^D_t}\le\dfrac{\sum_n\widetilde{P}^D_{n,t}}{\sum_n P^D_{n,t}}\le\overline{\Gamma^D_t},\right.\\ \widetilde{P}^D_{n,t}\in\left[P^D_{n,t}-\hat{P}^D_{n,t},P^D_{n,t}+\hat{P}^D_{n,t}\right]\end{array}\right\} \tag{48}$$

According to (48), the uncertain load varies within interval $\left[P^D_{n,t}-\hat{P}^D_{n,t},P^D_{n,t}+\hat{P}^D_{n,t}\right]$. To adjust the conservation level of the optimal solution, value of Γ^D (also called uncertainty budget) can be changed. Actually, with increasing Γ^D from 0 to 24, the conservation level of optimal solution increases and consequently, the hours that load of bus n can adopt its either lower or upper bounds, increases. Similar uncertainty set can be defined for solar power generation (U_G):

$$U_G=\left\{\begin{array}{l}\widetilde{P}^{PV}_{p,t}\in R^+\left|\underline{\Gamma^{PV}}\le\dfrac{\sum_p\sum_t\widetilde{P}^{PV}_{p,t}}{\sum_p\sum_t P^{PV}_{p,t}}\le\overline{\Gamma^{PV}},\right.\\ \widetilde{P}^{PV}_{p,t}\in\left[P^{PV}_{p,t}-\hat{P}^{PV}_{p,t},P^{PV}_{p,t}+\hat{P}^{PV}_{p,t}\right]\end{array}\right\} \tag{49}$$

with Γ^{PV} being the uncertainty budget of PV power generation. The uncertainty set for islanding event (U_I) is defined as follows:

$$U_I=\left\{\begin{array}{ll}\tilde{I}_t\in\{0,1\}\left|\sum_t\left(1-\tilde{I}_t\right)\le\ \Gamma^I,\right. & \forall t\in\left[T^{WRI}_s-1,T^{WRI}_e\right];\\ \sum_t I'_t=1,I'_t\ge\tilde{I}_{t-1}-\tilde{I}_t, & \forall t\in\left[T^{WRI}_s,T^{WRI}_e+1\right];\\ \tilde{I}_t=1, & \forall t\notin\left[T^{WRI}_s,T^{WRI}_e\right].\end{array}\right\} \tag{50}$$

Following a WRI, the MG may be disconnected from the external grid. Based on weather forecast data, the occurrence interval of the WRI, i.e.,$[T^{WRI}_s,T^{WRI}_e]$, can be predicted. However, the main challenge is to predict the exact islanding time and its duration. To cope with these challenges, the uncertainty budget Γ^I is applied to find the worst-case islanding time.

B. Two-Stage Robust Optimization Model

Considering the defined uncertainty sets, the two-stage robust optimization-based model can be formulated as follows:

$$\min_{x_t}\left\{\sum_{t\in\Omega_T}a^T_t x_t+\max_{U_D,U_G,U_I}\ \min_{y_t\in O(x_1,\ldots,x_T,i,d,g)}\sum_{t\in\Omega_T}b^T_t y_t\right. \tag{51}$$

$$C_t x_t\le c_t \tag{52}$$

$$O\left(x_1,\ldots,x_{24},i,d,g\right)=\left\{y_t\left|\begin{array}{l}H_t y_t\le h_t\\ G_t y_t\le L_t d_t-i_t x_t-E_t x_t-K_t g_t\\ N_t y_t\le w-M_t x_t\end{array}\right.\right\} \tag{53}$$

where, x and y are decision variables of normal and islanding operation modes, respectively. C, E, G, H, K, L, M, and N are auxiliary coefficients and a, b, c, h, and w are auxiliary parameters in compact robust model. i, d, and g are the uncertainty realization of islanding, load demand, and PV generation, respectively. In the proposed two stage robust model, the first-stage problem finds the robust energy and reserve scheduling of DGs, the energy scheduling of ESS and minimizes the total operation cost of MG considering the worst-case islanding realizations. After the first-stage decisions are determined, the worst-case islanding realization of MG under uncertainties can be computed by inner *max-min* model which essentially is a resiliency-oriented problem.

Equation (52) shows the feasible set for normal operation decision variables, i.e., constraints (12)-(27). The first inequality in (53) collects the constraints which merely involve islanding operation decision variables, i.e., constraints (7), (10), (30)-(37), and (40)-(47). The second inequality in (53) is specially selected to express constraints (28) and (29). Finally, the last inequality in (53) defines the compact form of (38) and (39).

C. C&CG Algorithm for Solving Two-Stage RO Based Model

The proposed *min–max–min* optimization problem of (51)-(53) cannot be solved by the commercial software packages. Thus, column-and-constraint generation algorithm, which is fully described in [21] , is used to efficiently solve the proposed robust model. In comparison to other algorithms such as Bender Decomposition (BD) algorithm [22], the C&CG algorithm can solve master problems with more variables and constraints in less iteration [23]. Furthermore, BD algorithm requires the sub-problem to be in linear format, but in C&CG algorithm this is not a requirement [21].

1) Master Problem (MP)

$$\min_{x_t,\varphi}\ \varphi \tag{54}$$

$$C_t x_t\le c_t \tag{55}$$

$$\varphi\ge\sum_{t\in\Omega_T}a^T_t x_t+\sum_{t\in\Omega_T}b^T_t y^{\vartheta}_t \tag{56}$$

$$H_t y^{\vartheta}_t\le h_t \tag{57}$$

$$G_t y^{\vartheta}_t\le L_t d^{\vartheta}_t-i^{\vartheta}_t x_t-E_t x_t-K_t g^{\vartheta}_t \tag{58}$$

$$N_t y^{\vartheta}_t\le w-M_t x_t \tag{59}$$

where, φ is an auxiliary variable and ϑ is the iteration index. The aim of the master problem is to find the optimal first-stage decision under those worst-case realizations which are achieved in the sub-problem. The master problem gives a lower bound for the two-stage robust optimization-based model (51)-(53).

2) Sub-Problem (SP)

The objective of the sub-problem is to find the worst-case realization over the defined uncertainty sets. For the first-stage optimal robust decisions, i.e., x^*_t, the sub-problem is as follows:

$$\eta\left(x^*\right)=\max_{d\in U_D,g\in U_G,i\in U_I}\ \min_{y_t\in L\left(x_1,\ldots,x_T,i,d,g\right)}\sum_{t\in\Omega_T}b^T_t y_t \tag{60}$$

$$H_t y_t\le h_t\qquad(\pi_t) \tag{61}$$

$$G_t y_t\le L_t d_t-i_t x^*_t-E_t x^*_t-K_t g_t\qquad(\gamma_t) \tag{62}$$

$$N_t y_t \le w - M_t x_t^* \qquad (\omega_t) \tag{63}$$

where, η is an auxiliary variable. π, γ, and ω are dual variables of constraints (61)-(63), respectively. The above *max-min* problem provides the upper bound for the two-stage robust optimization-based model (51)-(53). However, it cannot be optimized directly. Fortunately, since the sub-problem is a linear programming model, by using the duality theory, it can be written as follow:

$$\max_{\pi,\gamma,\omega,i,d,g} \sum_{t\in\Omega_T} \begin{Bmatrix} h_t^T \pi_t + \left(L_t d_t - I_t x_t^* - E_t x_t^* - K_t g_t\right)^T \gamma_t \\ + \left(w - M_t x_t^*\right)^T \omega_t \end{Bmatrix} \tag{64}$$

$$H_t^T \pi_t + G_t^T \gamma_t + N_t^T \omega_t = b_t \tag{65}$$

$$\pi_t \le 0, \gamma_t \le 0, \omega_t \le 0 \tag{66}$$

$$d_t \in U_D, g_t \in U_G, i_t \in U_I \tag{67}$$

By solving the derived equivalent formulation for the sub-problem, the worst-case realization over the uncertainty sets is determined in each iteration and corresponding constraints (56)-(59) are added to the master problem. The iterative process stops when the gap between the upper and lower bounds is less than a threshold. The flowchart of the proposed solution algorithm is shown in Fig. 2.

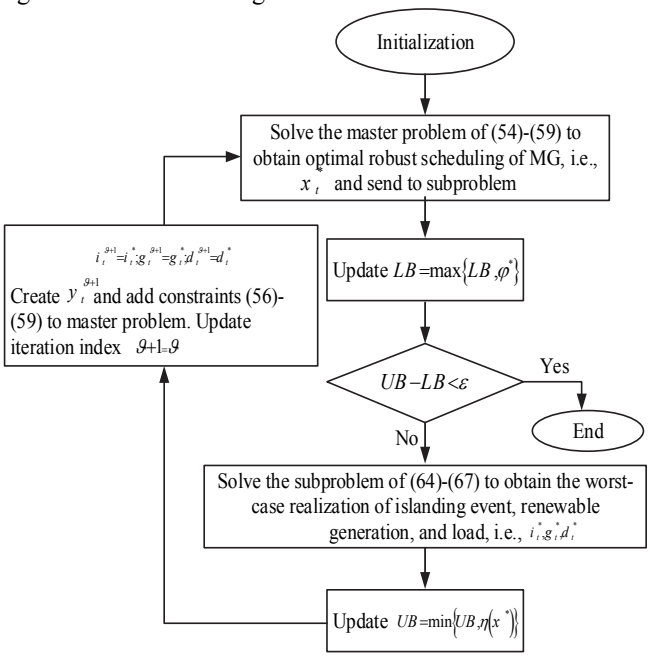

Fig. 2. Flowchart of the solution algorithm

V. Simulation Results

A. Data

The proposed model is applied to a typical MG test system as shown in Fig. 3. The MG includes five droop-controlled DGs where their technical and economic data are presented in Table I [15, 24]. The four PVs are the same type and their forecasted power generation is retrieved from [25]. The forecasted values of PV generation, scaled demand, and wholesale market price are shown in Fig. 4 [26]. The rated capacity of ESS is 1 MWh. The maximum, minimum, and initial SOC of ESS are 90%, 10%, and 90% of its capacity. The charging/ discharging power of ESS are limited to 0.2 MW. The values of λ^{ESS} and k_{SOC} are considered 106.5 \$/MWh and 0.15, respectively. It is assumed that the reactive power is technically assured. Meanwhile, the value of λ^{shed} is assumed 1000 \$/MWh [27]. The maximum permissible system frequency deviations in primary and secondary control intervals are set to 300mHz and 100mHz, respectively [18]. It should be noted that a 24-h scheduling horizon with 1-h time step is considered. However, any other scheduling horizon and step time can be selected based on the nature of the WRI and predicted data. The forecast error of PVs and loads are set to 10% and 5%, respectively. Meanwhile, the upper and lower values for uncertainty budgets of PVs and loads are considered 1.1 and 0.9, respectively.

The model is programmed in GAMS environment and solved using CPLEX solver on a computer with 4GB of RAM

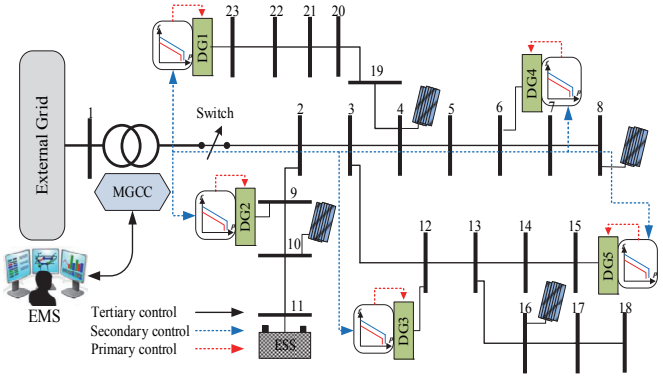

Fig. 3. Microgrid test system with hierarchical control levels

TABLE I
Technical and economic data of droop-controlled DGs

	DG1	DG2	DG3	DG4	DG5
$\overline{S^{DG}}$ (MVA)	4.68	4.16	4.16	4.16	4.27
$\overline{P^{DG}}$ (MW)	4.5	4	4	4	4.1
$\underline{P^{DG}}$ (MW)	1	0.75	0.75	0.75	1
α (\$)	27	25	25	28	26
β (\$/MWh)	87	87	87	92	81
λ^{RE} (\$/MWh)	11.4	9.025	9.025	9.7	10.7
$\lambda^{SU}/\lambda^{SD}$ (\$)	15/10	10/10	10/10	10/10	15/15
UR/DR (MW/h)	2/2	1.5/1.5	1.5/1.5	1.5/1.5	2/2
UT/DT (h)	2/2	2/2	2/2	2/2	2/2
mp (Hz/MW)	1	1	1	1.5	0.75
mq (kV/Mvar)	1.03	1.11	1.11	1.11	1.07

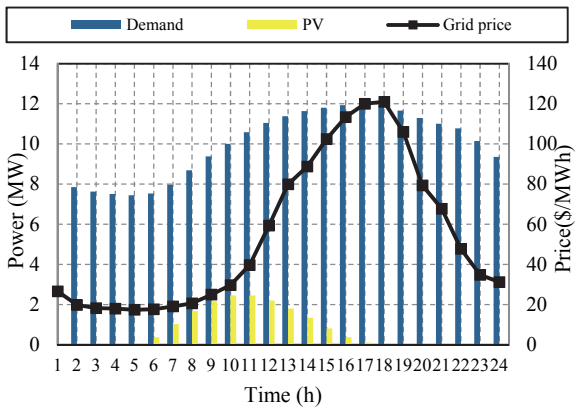

Fig. 4. Hourly forecasted values of demand, PV generation and market price

and Intel Core 2 Duo 2.50 GHz processor and has a runtime around 50 seconds which makes it practical even for rescheduling purposes in the day of operation (e.g., in 10 min intervals). The termination threshold for C&CG algorithm and the optimality gap for MILP solver are set to 0.05 and 0.01%, respectively.

B. Results and discussion

Based on the weather forecasts, it is assumed that WRI occurs between hours 3 to 12 and the MG may be islanded for 4 consecutive hours in this interval. Fig. 5 shows the MG day-ahead scheduling results of the proposed model. Likewise, the imported power from the external grid in a case where no preventive action is considered, is presented as a comparison benchmark. Results of simulated case study demonstrate that as the WRI starts at hour 3, the MG purchases less power from the grid and schedules its own DGs, although, they have higher prices than the grid. As mentioned, the robust model seeks the worst islanding interval, which in this case is between hours 8 to 11; therefore, at these hours the MG purchases the least power from the grid. Thus, if the MG is islanded in the real time operation, the lost power from the grid will be minimized which leads to zero load shedding. This strategy enhances the resiliency of the MG, dramatically. Note that during hour 12 to 16 (when the grid prices are relatively higher), the MGCC also prefers to further utilize DGs and reduce the imported power from the grid to minimize the total operation cost. Note that P^G in the islanding interval is not zero, since the day-ahead scheduling results are illustrated in Fig. 5 and the islanding may or may not occur in the real time operation of MG.

Following the islanding of MG, the primary, secondary, and reference powers of DGs are modified considering reserves to minimize the frequency deviation and load shedding. To clear this concept, the primary, secondary, and reference powers of DGs at hour 11 are shown in Table II. As can be seen in Fig. 5, following an islanding event, at hour 11, 1.32 MW imported power from the external grid is lost. Thus, the committed DGs should compensate this power shortage which leads to frequency deviation in primary and secondary intervals. According to (7), the primary frequency deviation can be calculated as follows:

$$\Delta f_{11}^{pri} = \frac{-(8.07-6.806)}{0.212+4} = -0.3 \quad Hz$$

The same analysis can be conducted for the secondary interval with the difference that in the secondary interval MGCC can also change the reference values of the DGs and compensate the power shortages.

Following the islanding of MG during hours 8-11, the lost imported power from the grid should be compensated by primary and secondary reserves. These reserves are shown in Fig. 6. As can be seen, due to the increase of load as well as PV generation during islanding interval, total scheduled reserves have an incremental behavior to cope with the uncertainties of load and PV generation. The MG frequencies following the deployment of the primary and secondary reserves are also shown in Fig. 6. As can be seen, frequency deviations can be securely regulated using the scheduled reserve capacities.

A Monte-Carlo simulation (MCS) has been conducted to evaluate the resiliency level of the proposed model. Without

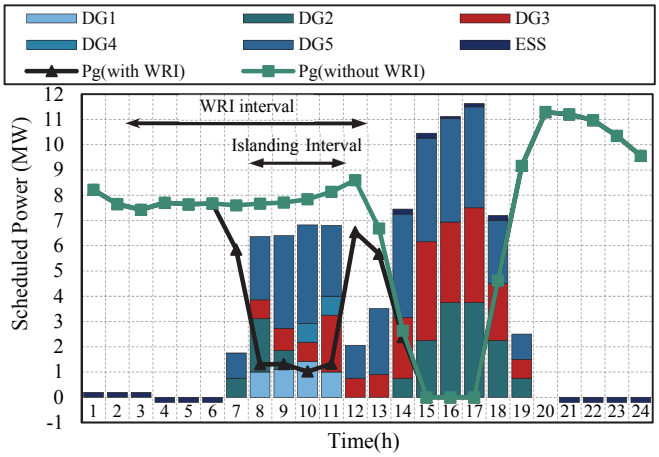

Fig. 5. Robust MG scheduling results

TABLE II
Values of primary, secondary, and reference powers of DGs at hour 11

	$P^{DG,pri}$ (MW)	$P^{DG,sec}$ (MW)	$P^{DG,ref}$ (MW)	$P^{DG,pre}$ (MW)	Δf^{pri} (Hz)	Δf^{sec} (Hz)
DG1	1.317	2	1.991	1		
DG2	0	0	0	0		
DG3	2.565	2.132	2.123	2.25	-0.3	-0.008
DG4	0.965	1.5	1.494	0.75		
DG5	3.221	2.5	2.488	2.806		

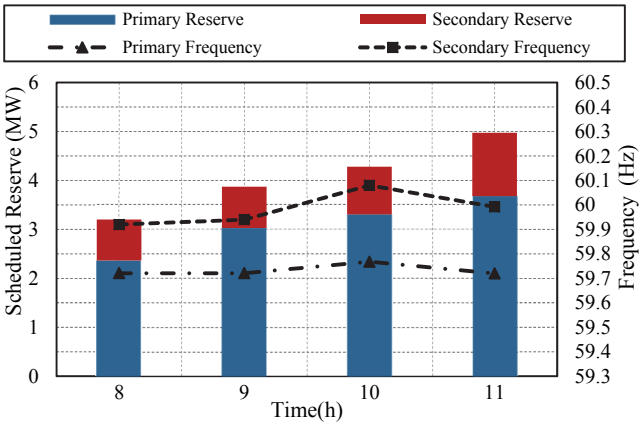

Fig. 6. Scheduled hourly primary and secondary reserve and MG frequency during islanding operation using the proposed robust model

loss of generality, it is assumed that the load, PV production, and occurrence interval of the WRI follow normal probability distributions where their mean value and standard deviations are $\mu_{n,t}^{D} = P_{n,t}^{D}$ and $\sigma_{n,t}^{D} = \hat{P}_{n,t}^{D}/3$ for load and $\mu_{p,t}^{PV} = P_{p,t}^{PV}$ and $\sigma_{p,t}^{PV} = \hat{P}_{p,t}^{PV}/3$ for PV power production and $\mu_{t}^{WRI} = I_t$ and $\sigma_{t}^{WRI} = \hat{I}_t/3$ for occurrence interval of the WRI. To keep the variation coefficient in MCS less than 1% , as defined in [28], 2000 simulations are performed. Total MG load shedding versus different normalized uncertainty budgets and the range of uncertain interval are shown in Fig. 7. As can be seen, with increasing the uncertainty budgets and the range of uncertainty intervals, total load shedding decreases significantly. Since resiliency is directly related to minimum load shedding [29], it can be concluded that the resiliency level of the proposed model increases. Therefore, the obtained results from MCS provides an effective criterion for MG operator to adopt suitable values

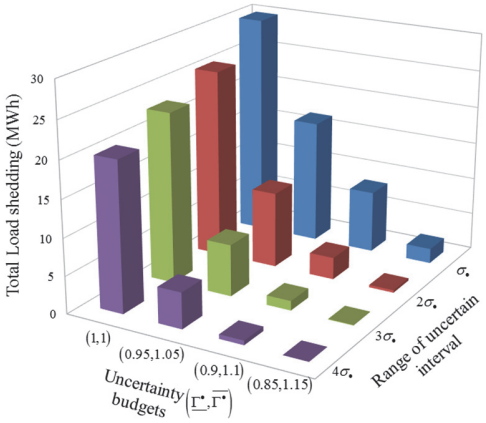

Fig. 7. Total load shedding for different robust scheduling using MCS

for uncertainty budgets and range of uncertainty intervals based on the resilience level before applying the proposed robust model.

Total operation cost of MG versus the adopted values for the normalized uncertainty budget and range of uncertainty interval is shown in Fig. 8. It is observed that with increasing the values of uncertainty budget and range of uncertainty interval, total operation cost of MG increases. This is due to the fact that the exchanged power with the grid is reduced and more expensive power and reserve capacities should be provided by DGs to assure a resilient operation against severe WRI events. It should be noted in Fig. 8, $(\underline{\Gamma}^{\bullet}, \overline{\Gamma}^{\bullet}) = (1,1)$ corresponds to deterministic scheduling of MG. As expected, total operation cost of MG by applying the proposed robust model is always higher than a deterministic model since extra payment should be made for accommodating higher resiliency levels.

In Fig. 9 variation of scheduled reserve and total operation cost with respect to elasticity of frequency dependent loads is presented. It implies that as the elasticity of loads increases, the needed total reserve capacity decreases which in turn reduces the total operation cost. This is due to the fact that when the frequency deviations increase the elastic loads reduce their consumption. Therefore, lower reserve should be scheduled and consequently, the total operation cost is decreased.

C. Comparative studies

A comparative study is presented in this section to evaluate the performance of the proposed model against methods of [30] and [11] (which are named as method 1 and method 2, respectively) in terms of cost-effectiveness, resiliency, and security improvement. In method 1, the uncertainties of PV output power, load, and islanding event are ignored and the MG scheduling is optimized to ensure that the system can be islanded for a predefined duration at every hour of the scheduling horizon. As the uncertainties play a key role in resiliency-oriented scheduling, in method 2, a set of scenarios that are a sequence of the uncertainties of PV output power, load, and islanding are generated using Monte Carlo simulations and the expected operation cost of MG is minimized through a two-stage stochastic optimization framework.

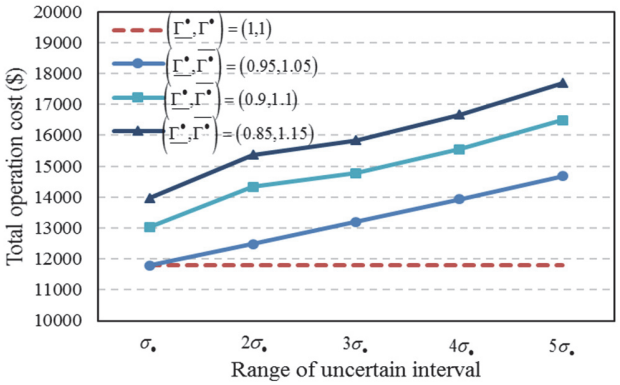

Fig. 8. Total operation cost of MG versus adopted values for the respective range and budget of uncertainty

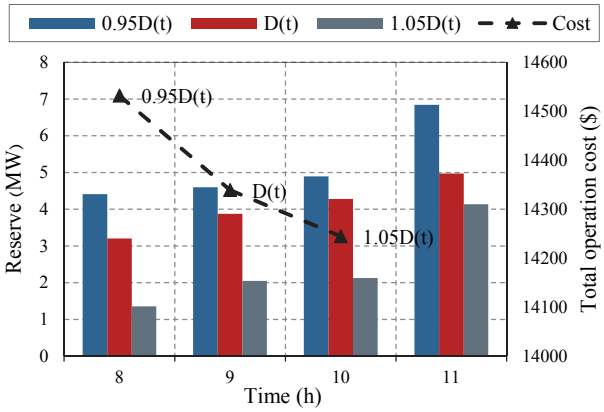

Fig. 9. Sensitivity of scheduled reserve and total operation cost to load frequency elasticity

In order to compare the above methods, the test system of Fig. 3 with given data is used. The predefined islanding duration in the first method is considered the same as our proposed model, i.e., 4 hours. In the second method, the prediction errors of load and PV output power are assumed to follow the normal distributions with standard deviations equal to 5% and 10% of the forecasted values, respectively which corresponds to the uncertainty intervals in our proposed model. Furthermore, a normal distribution with mean of four hours and standard deviation of one hour is considered for the islanding.

For the sake of comparison, the scheduling results achieved by each method are evaluated using MCS (under 2000 scenarios) against various realization of the uncertainties. To this end, the scheduling results are fed to the sub-problem of the proposed model and the total frequency deviations and load shedding are obtained for each scenario. Table III compares the methods in terms of cost-effectiveness, resiliency, and security. As it can be seen, the operation cost of the proposed model is 8.41% less than that of method 1 and slightly higher than the one obtained by method 2 (2.49% increment). The reason is that unlike the proposed robust model which finds the worst realization of uncertainties, method 1 is immunized against islanding for every hour of the scheduling horizon and method 2 only considers scenarios with high probabilities.

In Table III, insecure scenarios are those scenarios that result in violation of frequency constraints (i.e., (30) and (31)) for at

Table III
Comparison of the proposed model with methods of [30] and [11]

Comparison term	Method1	Method 2	Proposed model
Total operation cost ($)	15535	13971	14329
Number of insecure scenarios	37	123	8
Security (%)	98.15	93.85	99.60
Load shedding (MWh)	3.543	8.622	1.275

least one hour. Accordingly, the security is defined as the ratio of insecure scenarios to all examined scenarios. As it can be seen, due to consideration of hierarchical frequency control as well as robustness against the worst realization of uncertainties only eight insecure scenarios occur in the proposed model which indicate the highest level of security among the examined models. Additionally, since resiliency is directly related to load shedding, the proposed model provides the most resilient scheduling with the least load shedding.

VI. CONCLUSION

This paper proposed a two-stage robust optimization model for resilient operation of MGs in which hierarchical frequency control structure was formulated. The grid-connected and islanded operation problem of MG was decomposed by C&CG algorithm and uncertainties associated with renewable generation, load, and islanding events were addressed by the robust model. The simulation results demonstrated that by proper scheduling of droop-controlled DGs, the MGCC can minimize total operation cost of MG while acommodating sufficient primary and secondary reserves to restrict frequency deviations and avoid load shedding under the worst-case realization of islanding event. Moreover, a MCS was conducted to demonstrate the effectiveness of the proposed method in reducing load shedding and enhancing resiliency in different working scenarios. MCS could also be effectively used in decision-making of an MG operator to adopt suitable values for uncertainty budgets and range of uncertain intervals based on the resilince level before applying the proposed robust model.

APPENDIX

According to the droop control principles, the microgrid frequency and bus voltages could be regulated through active and reactive power management, respectively [18, 19]. In this paper, it is assumed that there is an analogous mechanism for the reactive power regulation which is performed in a decoupled way; thus, the voltage regulation requirements could be satisfied locally. To assure technically that reactive power demand of the MG is supplied, the proposed model can be updated with the following constraints:

$$Q_t^{shunt} + Q_t^{G} + \sum_{j \in DG} Q_{j,t}^{DG} = \sum_{n \in N} \tan\theta_{n,t} P_{n,t}^{D} \quad \text{(A1)}$$

where, Q^{shunt}, Q^{G}, and θ are the reactive power of shunt compensators, imported reactive power from external grid, and power angle. The reactive power provided by the converter-interfaced DGs and shunt compensators must be limited to their capacities as follows:

$$Q_{j,t}^{DG} \le \overline{Q_{j,t}^{DG}} \quad \text{(A2)}$$

$$Q_t^{shunt} \le \overline{Q_t^{shunt}} \quad \text{(A3)}$$

In day-ahead scheduling, since the converter-interfaced DGs are used to supply active power and reserve, the maximum reactive power capability of a DG is limited by the converter's rating (S^{max}) and its active power and reserve, as follows:

$$\overline{Q_{j,t}^{DG}} = \sqrt{(S_j^{max})^2 - \left(P_{j,t}^{DG} + R_{j,t}^{DG,pri} + R_{j,t}^{DG,sec}\right)^2} \quad \text{(A4)}$$

Note that the voltage of MG busses should be preserved in a secure range as follows [24]:

$$0.95pu \le V_{n,t} \le 1.05pu \quad \text{(A5)}$$

The voltages are calculated by implementing the linear power flow concept of [24]. The proposed model has been modified by considering the above constraints and simulated on the test system of Fig. 3. The technical data of the test system are presented in Table IV. It is assumed that the power factor of loads is 0.9 lag and no shunt compensator is installed in the MG test system. Other required technical data is also presented in Table I.

The reactive power dispatch is shown in Fig. 10. As can be seen, for example, during the islanding interval (i.e., hours 8-11) the needed reactive power is supplied by DGs. The share of each DG in reactive power compensation is determined based on the Q-V droop characteristic as presented in (2). Note that the reactive power production of DGs is limited to their maximum capability as indicated in (A4). Meanwhile, the voltage profile of the MG is illustrated in Fig. 11. As can be seen, the voltages of buses are preserved in the predefined secure range. It should be mentioned that since P-f and Q-V droop controls of converter-interfaced DGs are performed in a decoupled way, the energy and reserve scheduling results are similar to the case in which the reactive power is ignored.

TABLE IV
Technical data of MG test system

From/ to bus	Impedance (Ω)	End bus load (% of total load)	From/ to bus	Impedance (Ω)	End bus load (% of total load)
1-2	0.092+j0.047	0	12-13	1.468+j1.155	3.217
2-3	0.493+j0.251	5.361	13-14	0.541+j0.712	3.217
3-4	0.366+j0.186	4.825	14-15	0.591+j0.526	6.43
4-5	0.381+j0.191	6.434	13-16	0.746+j0.545	3.217
5-6	0.819+j0.707	3.217	16-17	1.289+j1.721	3.217
6-7	0.187+j0.618	3.217	17-18	0.732+j0.574	3.217
7-8	0.711+j0.231	10.723	4-19	0.164+j0.156	4.825
2-9	1.030+j0.740	10.723	19-20	1.504+j1.355	4.825
9-10	1.044+j0.740	3.217	20-21	0.409+j0.478	4.825
10-11	0.196+j0.065	3.217	21-22	0.708+j0.937	4.825
3-12	0.374+j0.123	2.412	22-23	0.451+j0.308	4.825

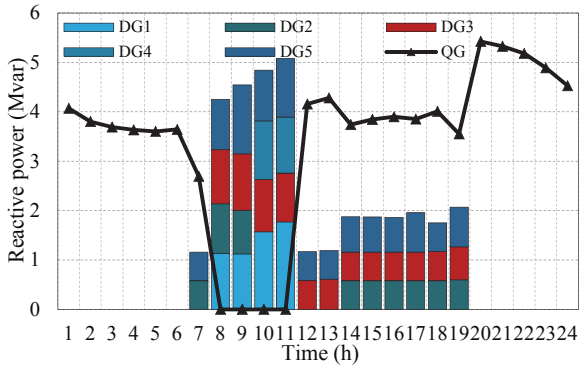

Fig. 10. Reactive power dispatch of MG

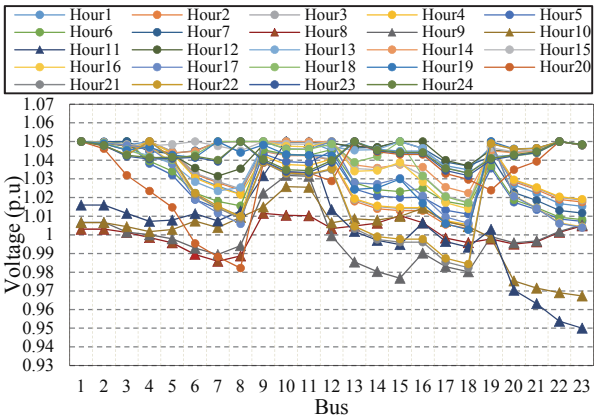

Fig. 11. Voltage profile of MG

REFERENCES

[1] Y. Wang, C. Chen, J. Wang, and R. Baldick, "Research on Resilience of Power Systems Under Natural Disasters—A Review," *IEEE Transactions on Power Systems,* vol. 31, pp. 1604-1613, 2016.

[2] M. Panteli, C. Pickering, S. Wilkinson, R. Dawson, and P. Mancarella, "Power System Resilience to Extreme Weather: Fragility Modeling, Probabilistic Impact Assessment, and Adaptation Measures," *IEEE Transactions on Power Systems,* vol. 32, pp. 3747-3757, 2017.

[3] "A Framework for Establishing Critical Infrastructure Resilience Goals," National Infrastructure Advisory Council (NIAC), Washington,DC,USA.

[4] M. Panteli and P. Mancarella, "The Grid: Stronger, Bigger, Smarter?: Presenting a Conceptual Framework of Power System Resilience," *IEEE Power and Energy Magazine,* vol. 13, pp. 58-66, 2015.

[5] T. Strasser, F. Andrén, J. Kathan, C. Cecati, C. Buccella, P. Siano, *et al.*, "A Review of Architectures and Concepts for Intelligence in Future Electric Energy Systems," *IEEE Transactions on Industrial Electronics,* vol. 62, pp. 2424-2438, 2015.

[6] Y. Xu, C. Liu, K. P. Schneider, F. K. Tuffner, and D. T. Ton, "Microgrids for Service Restoration to Critical Load in a Resilient Distribution System," *IEEE Transactions on Smart Grid,* vol. 9, pp. 426-437, 2018.

[7] A. Hussain, V. Bui, and H. Kim, "A Proactive and Survivability-Constrained Operation Strategy for Enhancing Resilience of Microgrids Using Energy Storage System," *IEEE Access,* vol. 6, pp. 75495-75507, 2018.

[8] A. Hussain, V. Bui, and H. Kim, "Optimal operation of hybrid microgrids for enhancing resiliency considering feasible islanding and survivability," *IET Renewable Power Generation,* vol. 11, pp. 846-857, 2017.

[9] H. Farzin, M. Fotuhi-Firuzabad, and M. Moeini-Aghtaie, "Enhancing Power System Resilience Through Hierarchical Outage Management in Multi-Microgrids," *IEEE Transactions on Smart Grid,* vol. 7, pp. 2869-2879, 2016.

[10] A. Gholami, T. Shekari, F. Aminifar, and M. Shahidehpour, "Microgrid Scheduling With Uncertainty: The Quest for Resilience," *IEEE Transactions on Smart Grid,* vol. 7, pp. 2849-2858, 2016.

[11] H. Farzin, M. Fotuhi-Firuzabad, and M. Moeini-Aghtaie, "Stochastic Energy Management of Microgrids During Unscheduled Islanding Period," *IEEE Transactions on Industrial Informatics,* vol. 13, pp. 1079-1087, 2017.

[12] M. H. Amirioun, F. Aminifar, and H. Lesani, "Resilience-Oriented Proactive Management of Microgrids Against Windstorms," *IEEE Transactions on Power Systems,* vol. 33, pp. 4275-4284, 2018.

[13] A. Khodaei, "Resiliency-Oriented Microgrid Optimal Scheduling," *IEEE Transactions on Smart Grid,* vol. 5, pp. 1584-1591, 2014.

[14] M. Farrokhabadi, C. A. Cañizares, and K. Bhattacharya, "Frequency Control in Isolated/Islanded Microgrids Through Voltage Regulation," *IEEE Transactions on Smart Grid,* vol. 8, pp. 1185-1194, 2017.

[15] N. Rezaei, A. Ahmadi, A. H. Khazali, and J. M. Guerrero, "Energy and Frequency Hierarchical Management System Using Information Gap Decision Theory for Islanded Microgrids," *IEEE Transactions on Industrial Electronics,* vol. 65, pp. 7921-7932, 2018.

[16] J. M. Guerrero, M. Chandorkar, T. Lee, and P. C. Loh, "Advanced Control Architectures for Intelligent Microgrids—Part I: Decentralized and Hierarchical Control," *IEEE Transactions on Industrial Electronics,* vol. 60, pp. 1254-1262, 2013.

[17] A. Milczarek, M. Malinowski, and J. M. Guerrero, "Reactive Power Management in Islanded Microgrid—Proportional Power Sharing in Hierarchical Droop Control," *IEEE Transactions on Smart Grid,* vol. 6, pp. 1631-1638, 2015.

[18] J. M. Guerrero, J. C. Vasquez, J. Matas, L. G. d. Vicuna, and M. Castilla, "Hierarchical Control of Droop-Controlled AC and DC Microgrids—A General Approach Toward Standardization," *IEEE Transactions on Industrial Electronics,* vol. 58, pp. 158-172, 2011.

[19] T. Greyard, "Overview of the Microgrid Concept and its Hierarchical Control Architecture," *International Journal of engineering research and technology,* vol. 6, 2016.

[20] J. Rocabert, A. Luna, F. Blaabjerg, and P. Rodríguez, "Control of Power Converters in AC Microgrids," *IEEE Transactions on Power* Electronics, vol. 27, pp. 4734-4749, 2012.

[21] B. Zeng and L. Zhao, "Solving two-stage robust optimization problems using a column-and-constraint generation method," *Operations Research Letters,* vol. 41, pp. 457-461, 2013.

[22] S. Dehghan, N. Amjady, and A. Kazemi, "Two-Stage Robust Generation Expansion Planning: A Mixed Integer Linear Programming Model," *IEEE Transactions on Power Systems,* vol. 29, pp. 584-597, 2014.

[23] Y. Guo and C. Zhao, "Islanding-aware robust energy management for microgrids," *IEEE Transactions on Smart Grid,* vol. 9, pp. 1301-1309, 2016.

[24] M. Mohiti, H. Monsef, A. Anvari-moghaddam, J. Guerrero, and H. Lesani, "A decentralized robust model for optimal operation of distribution companies with private microgrids," *International Journal of Electrical Power & Energy Systems,* vol. 106, pp. 105-123, 2019/03/01/ 2019.

[25] M. Mazidi, A. Zakariazadeh, S. Jadid, and P. Siano, "Integrated scheduling of renewable generation and demand response programs in a microgrid," *Energy Conversion and Management,* vol. 86, pp. 1118-1127, 2014/10/01/ 2014.

[26] "(2018, July. 1). New York Independent System Operator, online available at: http://mis.nyiso.com/public/P-2Alist.htm."

[27] H. Lotfi and A. Khodaei, "AC Versus DC Microgrid Planning," *IEEE Transactions on Smart Grid,* vol. 8, pp. 296-304, 2017.

[28] R. Billington and R. N. Allan, "Reliability evaluation of power systems," 1984.

[29] M. Panteli, D. N. Trakas, P. Mancarella, and N. D. Hatziargyriou, "Boosting the power grid resilience to extreme weather events using defensive islanding," *IEEE Transactions on Smart Grid,* vol. 7, pp. 2913-2922, 2016.

[30] A. Khodaei, "Microgrid Optimal Scheduling With Multi-Period Islanding Constraints," *IEEE Transactions on Power Systems,* vol. 29, pp. 1383-1392, 2014.

Maryam Mohiti received the B.Sc. and M.Sc. degrees from Sharif University of Technology, Tehran, Iran, in 2011 and 2013, respectively, and the Ph.D. degree in electrical engineering from the University of Tehran, Tehran, Iran, 2019. Her research interest includes microgrids operation, control, and protection, multiple microgrids, power system resilience, and application of power electronics in power systems.

Hassan Monsef received his B. Sc., M. Sc., and Ph. D. degrees in electrical and computer engineering from Sharif University of Technology, University of Tehran, and Sharif University of Technology, Tehran, Iran, in 1986, 1989, and 1996, respectively. He joined University of Tehran in 1996, where he is currently a Full Professor in the School of Electrical and Computer Engineering. Dr. Monsef has published more than 200 technical papers, two University of Tehran Press books in the areas of power system economics and renewable energy systems. He has been working closely with Iranian companies, assisting them in achieving technical and commercial success through research and new product development. He has authored/co-authored

more than 100 technical reports for the Iranian Electric Power Industries. Dr. Monsef has supervised more than 120 graduate students. Six of his PhD students found academic positions around world upon completion of their studies at University of Tehran. He is the founder of the Laboratory for Power System Operation and Planning Studies in the University of Tehran

Amjad Anvari-Moghaddam (S'10–M'14–SM'17) received the Ph.D. degree (Hons.) from University of Tehran, Tehran, Iran in 2015 in Power Systems Engineering. From 2015 until 2019 he was a Postdoctoral Research Fellow at Aalborg University, Denmark. Currently, he is an Associate Professor at the Department of Energy Technology, Aalborg University. His research interests include planning, control and operation of energy systems, mostly renewable and hybrid power systems with appropriate market mechanisms.

Dr. Anvari-Moghaddam serves as the GE/Associate Editor of the IEEE ACCESS, IET RENEWABLE POWER GENERATION, IEEE TRANSACTIONS ON INDUSTRIAL INFORMATICS, journal of FUTURE GENERATION COMPUTER SYSTEMS, journals of APPLIED SCIENCES, ELECTRONICS and SUSTAINABILITY. He is the recipient of 2020 DUO – India Fellowship Award, 2018 IEEE Outstanding Leadership Award (Halifax, Nova Scotia, Canada), the 2017 IEEE Outstanding Service Award (Exeter-UK) and the DANIDA research grant from the Ministry of Foreign Affairs of Denmark in 2018.

Hamid Lesani received the M.S. degree in power engineering from the University of Tehran, Tehran, Iran, in 1975 and the Ph.D. degree in electrical engineering from the University of Dundee, Dundee, U.K., in 1987. Then, he joined the Department of Electrical and Computer Engineering, University of Tehran, where he currently serves as a Professor at the Center of Excellence for Control and Intelligent Processing. His teaching and research interests is focused on design and modeling of electrical machines and power systems.